Reflection scanning near-field optical microscopy in ultrahigh vacuum

Stefan Hoppe,[a] Georgios Ctistis, Jens J. Paggel, and Paul Fumagalli
Freie Universität Berlin, Institut für Experimentalphysik, 14195 Berlin, Germany

A reflection scanning near-field optical microscope with polarization-sensitive light detection for operation in ultrahigh vacuum is presented. All necessary stages to reach the final goal of subwavelength resolution in magneto-optics are considered step by step, validating our approach and demonstrating the usefulness of the final instrument. A number of problems are attacked and discussed, but some are only treated to an extent necessary to bring the instrument to operation. Sub-λ resolution of a nonmagnetic polarization signal is demonstrated. © *2005 American Institute of Physics.* [DOI: 10.1063/1.1922789]

I. INTRODUCTION

Scanning near-field optical microscopy (SNOM) is a technique combining atomic-force microscopy (AFM)[1] with optical resolution beyond the diffraction limit.[2,3] Usually, an aluminum-coated optical fiber tip with subwavelength aperture is scanned across the sample surface. Mostly, the size of the probe is responsible for the resolution.[4] With increasing interest in small-scale magnetic properties of materials, a method allowing measurements of the local magnetization in an applied magnetic field is needed. Classical Kerr micro scopy is an appropriate technique as the light itself does not interact with the magnetic field. Only the magnetized sample manipulates the polarization state of the light. Optical microscopy is, however, limited in resolution due to the finite wavelength and the resulting diffraction limit. The optical near field is one way to extend the resolution beyond the fundamental limit of the wavelength of the light. An alternative approach is to use smaller wavelengths to resolve technologically interesting structure sizes and employ x-ray Kerr microscopy or related techniques.[5] We use SNOM to measure the magneto-optic Kerr effect (MOKE)[6–8] with a resolution beyond the diffraction limit.[9,10] If the fundamental properties of small magnetic aggregates or thin films are of interest, sample contamination is an issue. One reason is the chemical change of the sample surface through the absorbed layer (e.g., oxidation). This will modify the magnetic properties. Another reason is the change in topography that influences the optical measurement.[11] To circumvent this problem, our SNOM is part of an ultrahigh vacuum (UHV) system. All preparation and measurement is done at pressures of 1×10^{-9} mbar or less.

In this article, we describe the instrument and discuss all properties and features needed to measure magnetic properties with high spatial resolution in an applied magnetic field in UHV. On this route side effects such as tip–sample interaction and light-induced tip heating are also discussed.

II. INSTRUMENT DESCRIPTION

Figure 1 shows the schematic block diagram of the SNOM in reflection mode. It is composed of two parts; one for topographic and one for optical analytics. Three different modes of operation with coated fiber tips are generally possible: illumination with near-field light and collection of far-field light, illumination with far-field light and collection in the near-field, and both illumination and collection using the near field.[12–15] Another method to get subwavelength resolution with polarization contrast is the depolarization SNOM that uses uncoated fiber tips.[16–18] Here, we illuminate with near-field light and collect in the far field. For the optical part, linearly polarized light is coupled into a single-mode fiber. A frequency-doubled Nd: yttrium–aluminum–garnet laser with a wavelength of 532 nm is used as the light source. The light is polarized by a Glan prism with a polarization error of less than 10^{-6}. To use maximum intensity and flexibility, the polarization direction of the laser light is controlled by a $\lambda/2$ plate. The linearly polarized light is then coupled into a single-mode fiber by means of an aperture-matched microscope objective. However, the fiber influences the polarization of the light. To obtain linearly polarized light at the tip, a $\lambda/4$ plate is installed between the polarizer and coupler. With this, the light can be adjusted in such a way that it is exactly linearly polarized at the SNOM tip. This is necessary for avoiding field enhancements and polarization changes resulting from plasmons in the tip coating.[19]

The tip illuminates the sample and the far-field light emitted by the sample is collected with a spherical mirror. The sample is positioned close to the focal point in order that the light is reflected from the spherical mirror at near normal incidence, thus hardly disturbing the polarization.[20] The light collected is then focused and shaped to a nearly parallel beam by a system of lenses. Finally, it is analyzed by a combination of Glan polarizer and photoelastic modulator (PEM) which can be rotated. Detection of the light is done by a photomultiplier.[6,21] The quality of the light polarization and the stability of the polarization direction is discussed later.

To image the sample, the optical fiber tip needs to be scanned across the sample surface with high precision. The
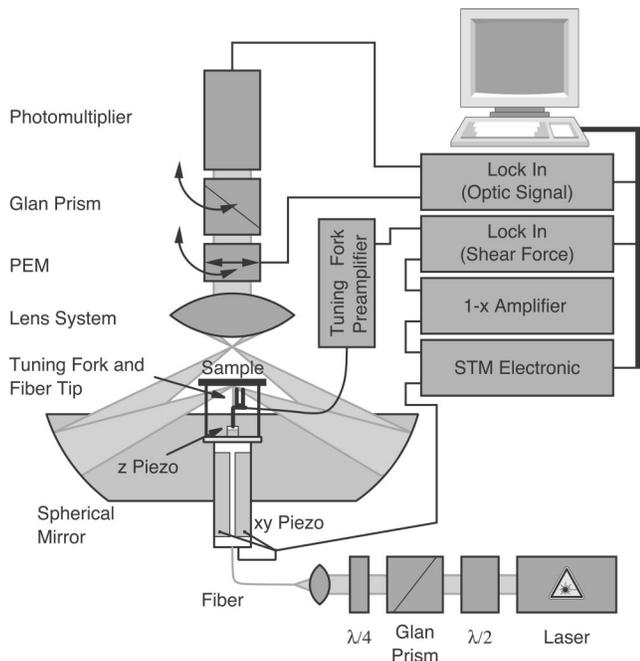
[a] Author to whom correspondence should be addressed; electronic mail: stefan.hoppe@physik.fu-berlin.de

FIG. 1. Block diagram of the MOKE-sensitive scanning near-field optical microscope.
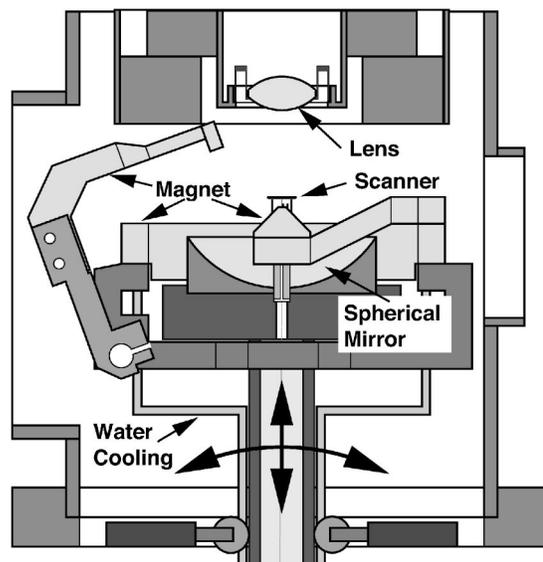

FIG. 2. Schematic image of the microscope in the UHV chamber in cross section. Indicated are the critical elements, such as scanner, magnet, lens, and mirror. The sample rests on the tiny scanner legs.

key ingredient is a sensitive tip–sample distance control. In general, this is obtained in SNOM by the use of a laterally vibrating tip and the shear–force interaction.[22] The optical fiber is attached to a piezoelectric tuning fork which is excited at its resonance frequency. The piezoelectric signal, which is proportional to the oscillation amplitude during approach, is analyzed by a lock-in amplifier and is fed into a feedback loop for distance control.[23] This way, surfaces of constant tuning-fork amplitude are measured. The scanner unit consists of two piezoelectric tube ceramics manufactured by Staveley Sensors Inc. The one carrying the sample is used for the $x-y$ scan while the z-position piezo carries the probe tip. The tip is not scanned in order to exclude polarization variations due to stress birefringence in the fiber caused by the bending of the fiber while scanning.

As mentioned above, the SNOM is part of an UHV system. The vacuum chamber is pumped with an ion getter pump and a titanium sublimator pump. Figure 2 pictures the main parts of the SNOM chamber as a cross section. The scanner is positioned in the center of the spherical mirror. An electromagnet is also included. The top magnet yoke is drawn in its open position which is used to transport the sample into the microscope. During measurement, it is closed yielding a gap of 5 mm. The unit scanner/mirror can be adjusted relative to the first lens of the focusing system even when the system is under vacuum. This adjustment accomplishes focusing the detection optics. The spherical lens also serves as the vacuum window as explained below.

A. Optical feedthrough

To realize the minimum complexity of the setup most optical components are outside the chamber at ambient conditions. The fiber and the first lens of the focusing system are used as vacuum–air interfaces. A special strain-free

feedthrough is needed to achieve good polarization stability. This is essential since the rotation of the light polarization due to stress birefringence exceeds the Kerr rotation by far. For the feedthrough, the fiber is threaded through a hypodermic needle and sealed with vacuum-compatible glue. The hypodermic needle itself is mounted in a CF16 flange. The setup is basically a fiber-optic feedthrough that minimizes mechanical strain on the fiber. The thick spherical lens is also glued into an assembly of two thin-walled cylinders. Differential thermal expansion this way stresses the cylinders, not the lens. The spherical lens itself is very uniformly stressed by the air pressure (only normal forces act on the glass surface). No large lateral variations of stress birefringence are observed in a test experiment confirming the polarization-preserving properties. The glue used in all cases is Varian Torr Seal.

B. The magnet

Since MOKE is an optical probe that can easily operate in an applied field, a magnet should be included in such a microscope. The influence of the magnet construction on the optical path has to be minimized and its design has to be compact to fit into an UHV chamber. At the same time, the applied field has to be as large as possible. These boundary conditions seem impossible to meet but distributing functionality leads to success. A photograph of the magnet implemented in the SNOM is shown in Fig. 3.

A long water-cooled Fe core is used. The windings are made in packages of 15, so the wire comes in contact with the core every 15 windings for a better cooling. The wire itself is insulated using glass-fiber tubing (Refrasil). From the right, an arm guides the magnetic field under the sample. The conical part is the bottom magnet yoke fully encompassing the scanner. The sample rests on three legs attached to the scanner's piezoelectric ceramic and penetrating the yoke. Only two of the three legs are visible. They are identified

FIG. 3. The SNOM with spherical mirror. Behind the mirror is the semicircular coil core made of pure iron. On the right hand side, the magnetic field is piped under the sample, on the left side over the sample.
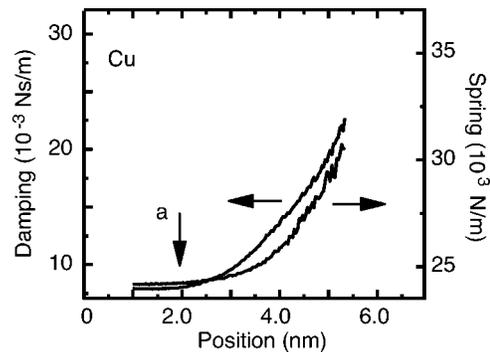

FIG. 4. Damping (left) and force (right) parameter of a harmonic-oscillator model fitted to the experimental approach curves of a probe tip approaching a Cu surface. The arrow *a* indicates the point of electrical contact.

through white ceramic balls acting as contact points. The arm on the left can be lifted and carries the upper magnet yoke. The maximum magnetic field amounts to $B=0.2$ T. The temperature increase of the magnet is less then $\Delta T=10$ K at the maximum field after 1 h. The Faraday effect in the fiber might contribute to the magneto-optic signal. The design of the magnet is, however, such that the tip is nearly not exposed to the magnetic field at all. The fiber is mainly inside the magnet yoke. We will demonstrate later that the optical setup is capable of detecting polarization rotations less than 0.01°.

C. The shear–force interaction

The distance between tip and sample is a sensitive parameter. In magneto-optic SNOM the detected light intensity is not only influenced by the tip–sample distance; it also depends on the light polarization. Unfortunately, the light transmission is very low as the local magneto-optic rotation is basically defined by the angle where the light intensity vanishes. The light intensity thus is not a reasonable measure for tip–sample distance. A common solution to the problem is to use the shear force between a probe tip and the sample. Shear force is the force acting on a laterally oscillating probe tip near a surface. The setup described here provides the stability and resolution to characterize the shear–force interaction on an atomic scale.[24,25] In contrast to a SNOM that is used in ambient conditions, in UHV there is no adsorbate film (like water) on the sample surface and the interaction is completely different from what is observed in ambient air conditions. At first, it is unclear if the shear–force interaction is useful at all for tip–sample distance control. This is discussed in depth in Ref. 26. The result of the detailed analysis is that the interaction takes place in mechanical contact to the sample and the interaction range is about 2 nm. This is in contrast to 10–20 nm at ambient conditions. The difference is probably due to the water film present on all surfaces at ambient conditions. The missing adsorbate film thus imposes

much stronger requirements on the stability and resolution of the tip–distance control in UHV SNOM than for work in air or inert atmosphere.

In Fig. 4, force and damping constants extracted from approach curves are plotted versus tip–sample position for Cu. Zero on the distance scale is chosen arbitrarily, and higher values correspond to a closer distance of the tip from the surface. At first, there is a sharp turn on of the interaction. The change in force and damping constant starts nearly simultaneously. *A priori*, the absolute distance between tip and sample is unknown. To extract this information, a bias voltage of 100 mV is applied between the Cu sample and the metal-coated tip. The arrow *a* in Fig. 4 shows the onset of ohmic resistance between tip and sample. Thus, shear–force interaction as applied to SNOM in UHV under our conditions is a modification of contact AFM.

III. LIGHT INDUCED THERMAL EXPANSION OF THE FIBER TIP

Our MOKE–SNOM operates with reflected light. The apex angle of the fiber tips has to be small to prevent shadowing of the converted far-field light by the tip itself. Also microstructured tips are not suitable due to their large base area and the related shadowing. The tips used in our instrument are, therefore, prepared by chemical etching in 40% hydrofluoric acid with a bromodecane protection layer. This recipe yields a cone angle of 29°.[27] A small apex angle directly converts to a long taper. The long taper has to be metal coated to avoid light leakage since the fiber taper destroys the light-guiding properties of the fiber. This means the light from the core of the fiber leaks into the cladding and would use the entire fiber in a waveguide-like manner in the limiting case. The illuminated spot in such a scenario would not correspond to the diameter of the aperture at the tip apex but still be on the order of the wavelength. The metal coating of the taper confines the light to the glass. At the apex of the tip, the coating has a small opening serving as the sub-λ light source (aperture). Since in the taper the dielectric light confinement is destroyed, energy dissipation in the form of heating of the taper is expected and observed.[28–30] In Fig. 5, tip and/or sample thermal expansion is measured for different intensities through the time response of the slow feedback signal for the shear–force distance control. As the shear–
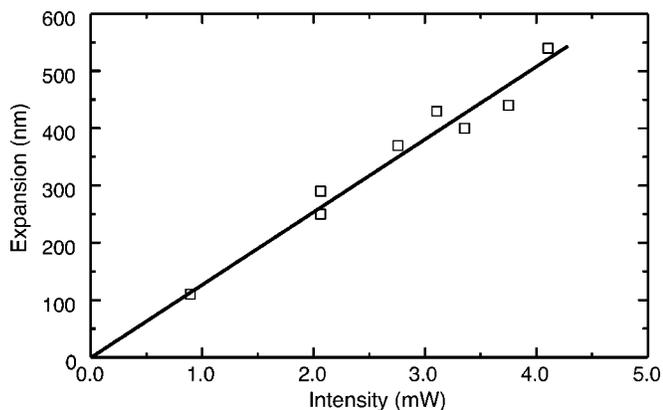
FIG. 5. Expansion of the fiber tip as a function of light intensity.

force control keeps the tip–sample distance constant, the thermal expansion of the tip is seen on the feedback signal. The expansion is plotted as a function of laser intensity. The result is a linear dependence with a slope of 127 nm/mW. Figure 6(a) shows the time dependence of the tip expansion for a laser power of 2.8 mW. The laser beam is blocked after 100 s. The linear plot shows a fast response. In the logarithmic plot [Fig. 6(b)], two dominating exponentials become evident. The decay times and the relative amount of the length change are independent of the laser intensity used. The fast one amounts to 80%, the slow one to 20% of the total length change. The noise in the logarithmic plot is due to limited digital resolution of the analog-to-digital converter used. The interpretation of the two contributions is still unclear and probably not very enlightening for the magneto-optic experiment.

IV. NEAR FIELD–FAR FIELD

After we have demonstrated that SNOM in UHV provides good control of the experiment, the question arises as to which distance to position the tip with respect to the sample for near-field optical experiments. In Fig. 7, the intensity is plotted versus the distance between tip and sample. The absolute position of the tip is well known from the force distance curves. The sample surface is located at 0 nm. There are three regions visible: (a) for large distances, far-field oscillations are observed due to interference between directly emitted and reflected light.[31] The period of the oscillation results from the laser wavelength and the detection angle θ between fiber and detector: $\lambda/(2 \cos \theta)$.[32] The detection angle is between 36° and 66° in our geometry. This is con-
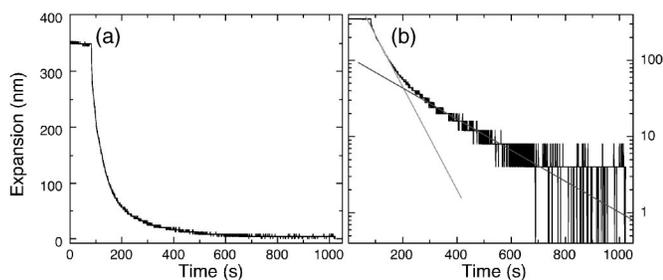

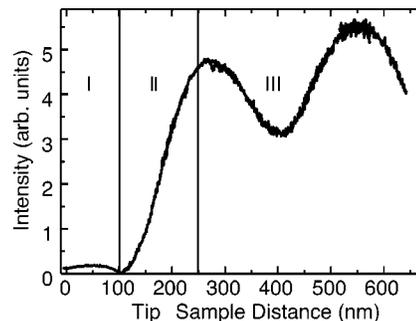FIG. 6. The elongation of the tapered tip vs time: linear (a) and logarithmic (b).

FIG. 7. Intensity of the reflected light as a function of tip–sample distance. The origin of the distance axis coincides with the point of contact between tip and sample.

sistent with what is shown in Fig. 7. (b) Between a distance of 250 and 100 nm, the tip shadows the reflected light and some light is coupled back into the fiber.[33] The total reflected intensity drops. (c) At distances closer than 100 nm, the intensity increases slightly from nearly zero. The light intensity does not drop to zero again, even for very small tip–sample distances. In close proximity of tip and sample, we thus clearly observe near-field light. This is exactly the distance where our feedback system positions the probe tip with respect to the sample surface. Optical signals measured at this tip position are near-field signals.

V. PERFORMANCE

A. Topographic

As shown before, the interaction between tip and sample is of rather short range under UHV conditions. This provides a vertical resolution on the atomic scale, i.e., single atoms cannot be imaged but features due to atomic steps on surfaces can be identified. To characterize the topographic resolution, a Si(111)–(7×7) sample with 4° miscut in direction of the [11-2] azimuth is prepared by direct current heating to about 1200 °C. A faceted surface is formed with facets of 8 nm in height and a width of 130 nm.[34] To protect the surface, the sample is covered by 0.5 nm Pt. Figure 8 pictures a topographic scan in a 3D representation. The z scale is greatly exaggerated. The Pt only covers the surface but leaves the facet structure unchanged. At the top edge, a smaller facet leaves a larger one. This smaller facet is used to analyze the topographic resolution of the image. The white line indicates the position of a line scan shown in Fig. 8(b).

This line scan shows that the vertical resolution of the instrument is on the order of a few Å and that the lateral is better than 10 nm. This is a remarkable resolution for a SNOM with fiber tip in shear–force detection mode. In contrast to conventional AFMs, the curvature of the tip apex of the glass–fiber tips is on the order of 100 nm.

B. Optic

In the preceding sections, we have demonstrated that we have built a low-resolution AFM for operation in UHV. The optical characterization of the microscope is discussed in this section. In Fig. 9, a so-called V curve measured in far-field mode is plotted. A V curve is obtained when measuring the
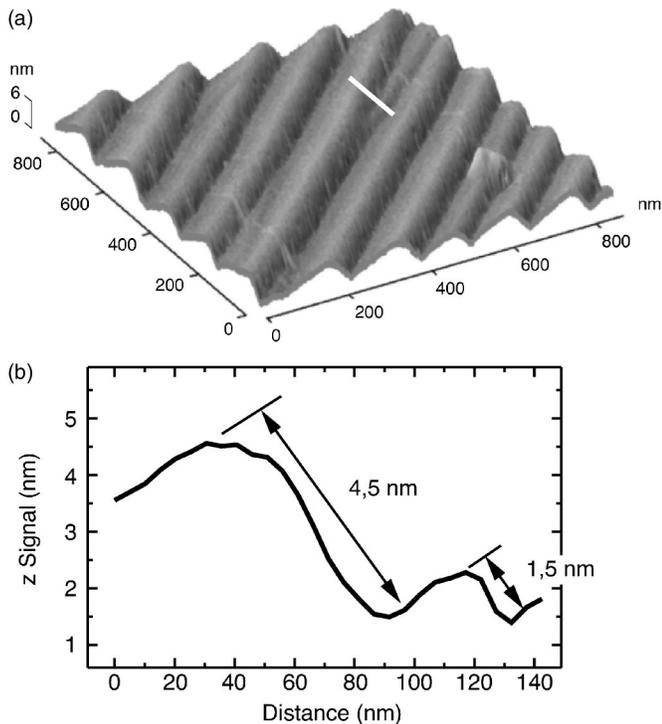
FIG. 8. (a) Pseudo-3D representation of a topographic scan of a faceted Si(111) surface with a defined miscut. The white line at the top corner indicates the position of a line scan analyzed in (b) and (b) line-scan representation of the section indicated in (a).

absolute value of the lock-in amplitude at twice the PEM frequency as a function of the angle of the analyzing unit with respect to the incident polarization. The analyzing unit consists of a PEM combined with a polarizer mounted at 45° with respect to the PEM axis. Both are rotated simultaneously.[35] A V curve contains of about 1000 data points. Two straight lines are fitted to the experimental data in a consistent way. The finite time constant of the lock-in amplifier shifts the minimum of the individual V curves. To obtain the correct rotation angle for the Kerr rotation, the V curve is measured in both directions and the angle for the minimum amplitude is averaged. The maximum deviation can be estimated by two parallel lines enveloping the data
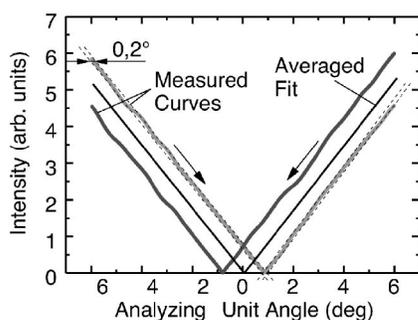

FIG. 9. Raw data of the V curves that are used to determine the Kerr-rotation angles in the MOKE experiment. Two measurements, back and forth, are shown together with the averaged fit. The target for every individual measurement is the angle corresponding to the cusp in the V curve. The angles of the cusp acquired as a function of applied field yield the Kerr loop. The light intensity obtained at a fixed angle of the PEM analzyer unit generates—in the absence of other effects—a map of the magnetic domains.
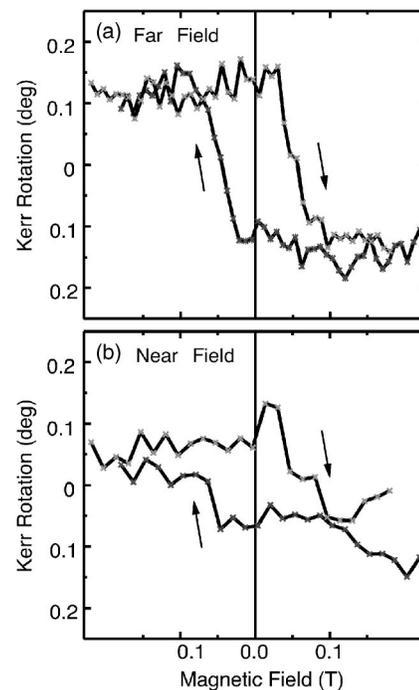

FIG. 10. (a) Far field and (b) near field hysteresis measurements on a CoPt multilayer.

points within each individual V curve (dashed lines in Fig. 9). This error amounts to about 0.2°. The precision obtained is, however, much better as will be evident in Fig. 10 showing Kerr loops.

Next, Kerr loops are shown in the far field [Fig. 10(a)] and the near-field [Fig. 10(b)]. As a reference sample, a CoPt multilayer with 10×0.3 nm Co and 1.0 nm Pt on a buffer of 10 nm Pt is used.[36] Every data point corresponds to a minimum of the V curve at that particular magnetic field. In Fig. 10(a), this is done in the far-field regime with a tip–sample distance of about 1 mm. The scatter of the Kerr-rotation measurement is about 0.05°, which is a more realistic value for the resolution of the optical setup. A nearly rectangular hysteresis curve is seen. The magnetization curve is consistent in coercive field and rotation magnitude with data obtained on a classical Kerr spectrometer. The Kerr rotation is 0.28° and the coercive field is 0.05 T. Figure 10(b) shows the near-field hysteresis loop in shear–force contact. The Kerr rotation observed is about half of the far-field value. A hysteresis is clearly visible confirming that local hysteresis curves are thus obtainable. Signal-to-noise ratio is, however, deteriorated with respect to the far-field value.

Finally, magneto-optics has to be combined with the scanning capabilities of the SNOM. Figure 11(a) shows an image of the magneto-optic contrast of an Fe garnet doped with rare-earth elements ([EuTm$_2$Ca]Ge$_{0.4}$). The light/dark contrast corresponds to a Kerr-rotation angle of a few tenths of a degree. The domains are, however, very large. This is a sample property. The image proves, nevertheless, that the microscope is capable of measuring small Kerr-rotation angles in order to image different magnetic domains. The sub-λ resolution, on the other hand, is shown in Fig. 11(b) where the magneto-optic contrast of the CoPt multilayer of Fig. 10 is shown. Rich structure with subwavelength resolu-
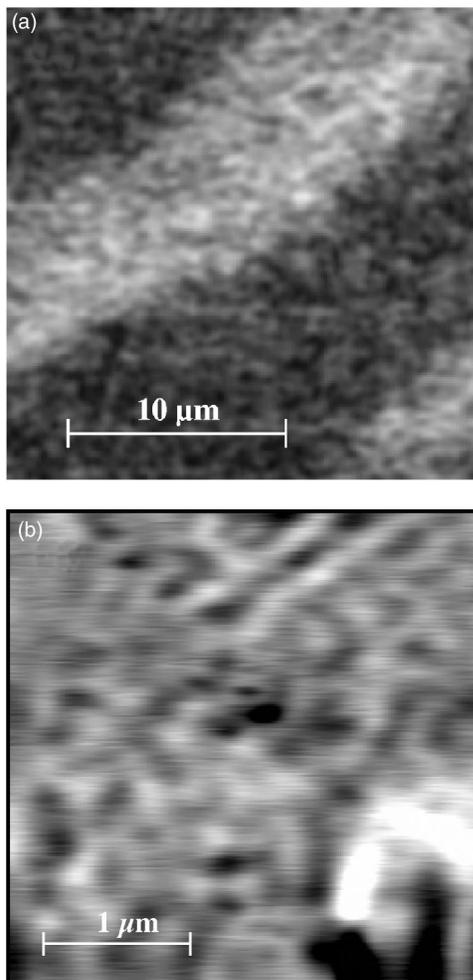
FIG. 11. Images employing polarization contrast: (a) magneto-optic contrast of a rare-earth doped Fe–garnet sample. Because the garnet is transparent, the contrast is thus at least partially due to the Faraday effect. (b) Polarization-dependent image of a CoPt multilayer. The polarization contrast corresponds to about 4° and is most likely due to stress birefringence. The underlying domain pattern cannot be resolved.

tion is observed. Disappointment arises when the rotation angles are discussed: the observed contrast corresponds to rotation angles of more than 4°. This is much larger than the Kerr rotation measured in the hysteresis loops in Fig. 10. The contrast is, therefore, not of magneto-optic origin but generated by stress birefringence. This is easily verified as the polarization contrast is independent of the applied magnetic field. In Fig. 10(b), we had demonstrated that the magneto-optic signal is present. It must be superimposed on the stress-induced signal. The magneto-optic signal is, however, about 2 orders of magnitude smaller. Hence, the extraction of the magneto-optic information by image subtraction is very difficult. Nevertheless, sub-λ resolution in the polarization contrast is evident. An alternative approach by Meyer *et al.* using the Sagnac effect eliminates the influence of nonmagnetic contributions.[37] Their approach, however, does not operate using near-field light and is therefore limited to about λ/3 in resolution.

In contrast our near-field optical microscope with its polarization-sensitive detector and built-in magnet works as we have shown above in the optical near field regime. The field during imaging can reach 0.2 T. We demonstrate topographic resolution on the atomic length scale. Polarization contrast with subwavelength resolution is observed. The resolution for the rotation angle of the light polarization is about 0.05°. All ingredients for subwavelength imaging of magneto-optic properties of nontransparent samples are therefore successfully demonstrated. A strong, strain-induced birefringence signal obstructs observation of magnetic contrast in some samples as, e.g., CoPt multilayers. Applying an image-subtraction technique in order to reduce the birefringence signal should improve performance even for such samples.

[1] G. Binnig, C. F. Quate, and C. Gerber, Phys. Rev. Lett. **56**, 930 (1986).
[2] H. Heinzelmann and D. W. Pohl, Appl. Phys. A **59**, 89 (1994).
[3] E. Betzig and J. K. Trautman, Science **257**, 189 (1992).
[4] B. Hecht, Ph.D. thesis, Philosophisch—Naturwissenschaftliche Fakultät der Universität Basel, 1996.
[5] R. Medenwaldt and E. Uggerhøj, Rev. Sci. Instrum. **69**, 2974 (1998).
[6] P. Fumagalli, A. Rosenberger, G. Eggers, A. Münnemann, N. Held, and G. Güntherodt, Appl. Phys. Lett. **72**, 2803 (1998).
[7] E. Betzig, J. K. Trautman, R. Wolfe, E. M. Gyorgy, P. L. Finn, M. H. Kryder, and C. H. Chang, Appl. Phys. Lett. **61**, 142 (1992).
[8] T. J. Silva and S. Schultz, Rev. Sci. Instrum. **67**, 715 (1996).
[9] A. Harootunian, E. Betzig, M. Isaacson, and A. Lewis, Appl. Phys. Lett. **49**, 674 (1986).
[10] D. Pohl, W. Denk, and M. Lanz, Appl. Phys. Lett. **44**, 651 (1984).
[11] A. Rosenberger, A. Münnemann, F. Kiendel, G. Güntherodt, P. Rosenbusch, J. A. C. Bland, G. Eggers, and P. Fumagalli, J. Appl. Phys. **89**, 7727 (2001).
[12] G. Eggers, A. Rosenberger, N. Held, A. Münnemann, G. Güntherrodt, and P. Fumagalli, Ultramicroscopy **71**, 249 (1998).
[13] J. A. Cline and M. Isaacson, Ultramicroscopy **57**, 147 (1995).
[14] J. Ferber, U. C. Fischer, N. Hagedorn, and H. Fuchs, Appl. Phys. A: Mater. Sci. Process. **69**, 581 (1999).
[15] W. A. Atiaa, S. Pileveara, A. Güngörb, and C. C. Davisa, Ultramicroscopy **71**, 379 (1998).
[16] G. v. Freymann, Th. Schimmel, M. Wegener, B. Hanewinkel, A. Knorr, and S. W. Koch, Appl. Phys. Lett. **73**, 1170 (1998).
[17] G. v. Freymann, M. Wegener, and Th. Schimmel, Surf. Interface Anal. **27**, 499 (1999).
[18] M. Schüttler, M. Leuschner, and H. Giessen, Jpn. J. Appl. Phys., Part 1 **38**, 1463 (1999).
[19] A. Bouhelier, J. Renger, M. R. Beversluis, and L. Novotny, J. Microsc. **210**, 220 (2002).
[20] S. Hoppe, Ph.D. thesis, Freie Universität Berlin, 2004.
[21] T. J. Silva, S. Schultz, and D. Weller, Appl. Phys. Lett. **65**, 658 (1994).
[22] K. Karrai and R. D. Grober, Appl. Phys. Lett. **66**, 1842 (1995).
[23] M. Lippitz, M. Schüttler, H. Giessen, M. Born, and W. W. Rühle, J. Appl. Phys. **86**, 100 (1999).
[24] M. Leuschner, M. Schüttler, and H. Giessen, J. Microsc. **202**, 176 (2001).
[25] M. Schüttler, M. Leuschner, M. Lippitz, W. W. Rühle, and H. Giessen, Jpn. J. Appl. Phys., Part 1 **40**, 813 (2001).
[26] S. Hoppe, G. Ctistis, J. J. Paggel, and P. Fumagalli, Ultramicroscopy **102**, 221 (2005).
[27] P. Hoffmann, B. Dutoit, and R.-P. Salathé, Ultramicroscopy **61**, 165 (1995).
[28] D. I. Kavaldjiev, R. Toledo-Crow, and M. Vaez-Iravani, Appl. Phys. Lett. **67**, 2771 (1995).
[29] C. Lienau, A. Richter, and T. Elsaesser, Appl. Phys. Lett. **69**, 325 (1996).
[30] L. Thiery and M. Marini, Ultramicroscopy **94**, 49 (2002).
[31] C. Obermüller, K. Karrai, G. Kolb, and G. Abstreiter, Ultramicroscopy

61, 171 (1995).

[32] C. Durkan and I. Shvets, J. Appl. Phys. **83**, 1837 (1998).

[33] O. Bergossi, M. Spajer, and P. Schiavone, Ultramicroscopy **61**, 241 (1995).

[34] R. S. Becker, J. A. Glovchenko, E. G. McRae, and B. S. Swartzentruber, Phys. Rev. Lett. **55**, 2028 (1985).

[35] G. Eggers, A. Rosenberger, N. Held, and P. Fumagalli, Surf. Interface Anal. **25**, 483 (1997).

[36] D. Weller, H. Notarys, T. Suzuki, G. Gorman, T. Logan, I. McFadyen, and C. Chien, IEEE Trans. Magn. **28**, 2500 (1992).

[37] G. Meyer, T. Crecelius, A. Bauer, I. Mauch, and G. Kaindl, Appl. Phys. Lett. **83**, 1394 (2003).